Abnormal WC crystal growth from liquid Co flux occurs via eta phase decomposition

Maxim Vreeswijk [a,b], Alexandre Kot [a], Finn Giuliani [a], Samuel Humphry-Baker [a]

[a] *Department of Materials, Imperial College London, Prince Consort Road, London, SW7 2BP, UK*
[b] *The Department of Materials Science and Metallurgy, University of Cambridge, 27 Charles Babbage Road, Cambridge, CB3 0FS, UK*

The growth mechanism of large WC crystals from a liquid Co-based flux is identified. This is achieved by systematically varying the growth temperature and Co content from 1200-1400 °C and 70-83 at.% respectively. Crystal growth was characterised using metallography and X-ray diffraction. The WC grains were bimodally distributed, consisting of a smaller (10-20 μm) population of grains, which nucleated homogenously from the liquid, and a secondary population of abnormally large grains, several millimetres in size. The abnormal grains nucleated on the $(W,Co)_6C$ eta phase, and subsequently consumed it through a carburisation reaction. The size of abnormal grains was enhanced by adopting the eutectic composition, such that the first solid phase to form was the eta phase, whilst at the same time undercooling immediately below the eta→WC transformation temperature, at ~1300°C. This growth mechanism could be exploited for a variety of metal carbides with similarly sluggish diffusion rates.

Keywords: Crystal growth, abnormal grain growth, eta phase, tungsten carbide

1. Introduction

WC-based composites consisting of a metallic matrix and WC particles are widely applied in metal-cutting and rock-drilling applications [1]. The matrix is usually Co, but sometimes Ni or Fe-based. Enhancing the tool longevity in such applications requires optimisation of properties such as the wear resistance, creep resistance, and fracture toughness [2]. Improving these parameters requires an understanding of the properties of its constituent phases, which, for WC, are highly anisotropic [3]–[6]. Therefore, the measurement of their orientation dependence requires large single crystals of high quality to be produced.

Single crystals are particularly helpful when studying creep resistance. The dominant creep deformation mechanism at high strain rates is grain boundary sliding (GBS) [7], [8] During GBS the WC/WC grain boundaries are infiltrated by Co, allowing them to slide past one another [9], [10]. Such infiltration is controlled by the work of separation of WC/WC GB's. First principles calculations [11], [12] suggest this work is increased by common grain growth inhibitors, such as V, Ti, Zr, Nb and Cr [13], [14], however this remains to be measured experimentally. Micro-pillar [15]–[17], micro-cantilever [18], [19] and micro-dual cantilever beam tests [20]–[23], could enable such measurements. However, application of these methods to individual interfaces requires very large grain sizes exceeding 100 μm.

Such grain sizes are not achievable using typical processing routes for WC-Co composites. This is because grain growth during conventional liquid phase sintering, in which the binder content is typically 3-15 wt.%, densification is dominated by the solution-reprecipitation mechanism [24]. The grain size during this process is governed by sluggish cubic-order grain growth kinetics [6], [25], [26], typically plateauing at 10 μm or so.

A more successful method for extensive grain growth is processing from a fully liquid phase [3], [27]. This can be achieved using high temperatures and/or cobalt contents exceeding

80 at.%. Takahashi and Freise [3] applied such melt solidification by slowly-cooling a WC-83Co composite from 1600 °C to obtain mm-sized grains. Later, Gerk and Gilman [27] repeated this technique at the stoichiometry WC-82Co. In both studies, WC followed faceted growth; the three-fold symmetry of the hexagonal crystal structure leads to fastest growth in the prism ($[1\bar{1}00]$-type) directions and slow growth in the $\langle 0001 \rangle$ basal directions. The resulting growth shape is a hexagonal prism, which eventually grows into a triangular one [5].

Despite the successful growth from the liquid in Refs. [3] and [27], neither detail the solidification processes, meaning the mechanisms of growth remain poorly understood. Fig. 1 shows the pseudo-binary phase diagram for WC-Co, revealing that at intermediate Co contents (~40-75 at%), WC is the first solid to form from upon cooling from the liquid. However, at the compositions studied by Refs [3] and [27], indicated by red and blue tie-lines, the $(W,Co)_6C$ phase [28], [29], hereafter referred to as η-phase, would also likely have formed, since it is stable between 1240 and 1450 °C when the W:C ratio is unity [30]. However, the η-phase was not mentioned in either study, therefore its role in growth from the liquid remains unclear.

Here we have systematically studied such η-phase formation, and its relation to abnormal WC growth, by varying the growth stoichiometry and temperature. We show that abnormally large WC grains can only be grown via decomposition of the η-phase. We explore the conditions under which such abnormal growth can be optimised.

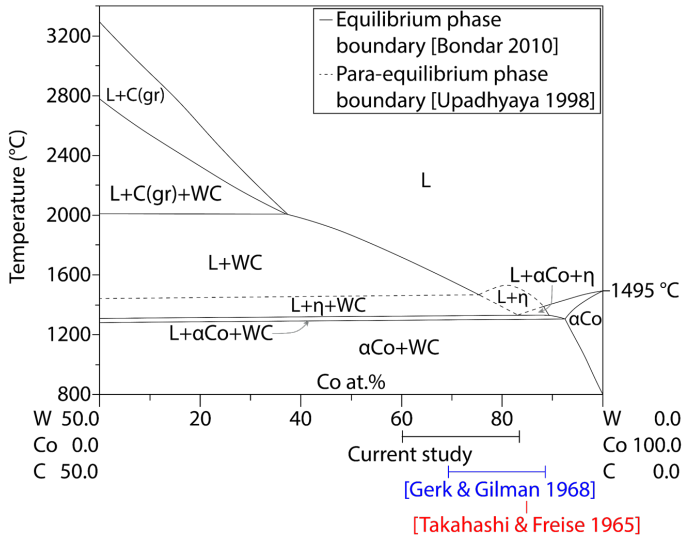

Fig. 1. Pseudo-binary phase diagram for the WC-Co system. Equilibrium phase boundaries (solid lines) are taken from Refs. [31], [32]. The para-equilibrium phase boundaries (dashed lines) are from Ref. [30]. Compositions from previous growth studies (tie lines) from Refs. [3], [27].

2. Experimental methods

Ternary WC-Co powder mixtures were fabricated with Co contents of 70-83 at.%, i.e. up to the eutectic point in Fig. 1. The exact compositions are listed in table 1. The powders were handled and weighed in a glovebox under pressurised argon. The WC material (SECO Tools AB) had an average cross-sectional grain size of 2.36 ± 0.2 μm. This value was measured using the linear intercept method following [33] to calculate the projected area of each grain, which was then converted into its equivalent cross-sectional grain size by multiplying it by a factor of $2/\pi$. A square raster was used, with a spacing large enough such that each grain would not be crossed more than twice. The mean is given as the sum of the measured intercept lengths, divided by the number of intercepted grains. Excessively large grains (>100 μm) were

54 measured with a coarser secondary raster. The Co powder was gas atomised (Sigma-Aldrich),
55 had a < 0.2% trace metal content, and an average grain size of 2 μm. 30-45 g of powders were
56 sealed in Nalgene containers, and then mixed in a turbular mixer for 20 h.

57 **Table 1.** Powder mixture compositions. Mixture names represent the atomic % Co. WC makes up the
58 remainder.

Mixture name	WC (wt.%)	Co (wt.%)
WC-70Co	58.7	41.3
WC-72.5Co	55.7	44.3
WC-75Co	52.5	47.5
WC-77.5Co	49.0	51.0
WC-80Co	48.3	51.7
WC-83Co	40.0	60.0

59 After mixing, the powders were poured into lid-topped alumina crucibles and heat
60 treated in a graphite-lined sinter furnace with graphite heating elements (FCT Systeme GmbH)
61 operated in vacuum. All compositions underwent heat treatment T1200, where samples were
62 heated to 1600 °C, held isothermally for 20 hours, cooled at 1 °C/min to 1200 °C, and held
63 again isothermally for 10 hours before furnace cooling to room temperature. Additionally, The
64 WC-83Co mixture was heat treated using heat treatments T1300 and T1400, in which the
65 secondary isothermal holds were 1300 °C and 1400 °C, respectively. The pseudo-binary WC-
66 Co phase diagram in Fig. 1 shows that during the primary 1600 °C hold, all samples were fully
67 liquid, while the T1200, T1300 and T1400 secondary holds were in the Co+WC, the
68 L+Co+WC, and the L+η phase fields, respectively.
69 After heat treatment, samples were cut, ground, and polished up to 0.05 μm colloidal
70 silica. X-ray diffraction (XRD) patterns were collected using a Bruker D2 phaser, CuK_α source
71 (λ=0.15418 nm), step size 0.0330° and time per step 0.707s. Scanning electron microscopy
72 (SEM) images, were collected using a Jeol JSM-6010LA microscope in secondary electron
73 (SE) mode. Stereology of the SEM images indicated that during the heat treatments there was
74 minimal Co evaporation, as the atomic fractions of Co were consistently with 0.9-2.7 % of the
75 nominal value.

3. Results and discussion

76 Fig. 2 shows the samples grown from sub-eutectic compositions (70-80 at.% Co). Part
77 (a) shows XRD patterns, which exhibit the WC and high temperature FCC α-Co in all samples.
78 The scanning electron microscopy (SEM) images, collected using a Jeol JSM-6010LA
79 microscope in secondary electron (SE) mode show three distinct populations of WC grains
80 labelled 1-3 in Fig. 2(b).

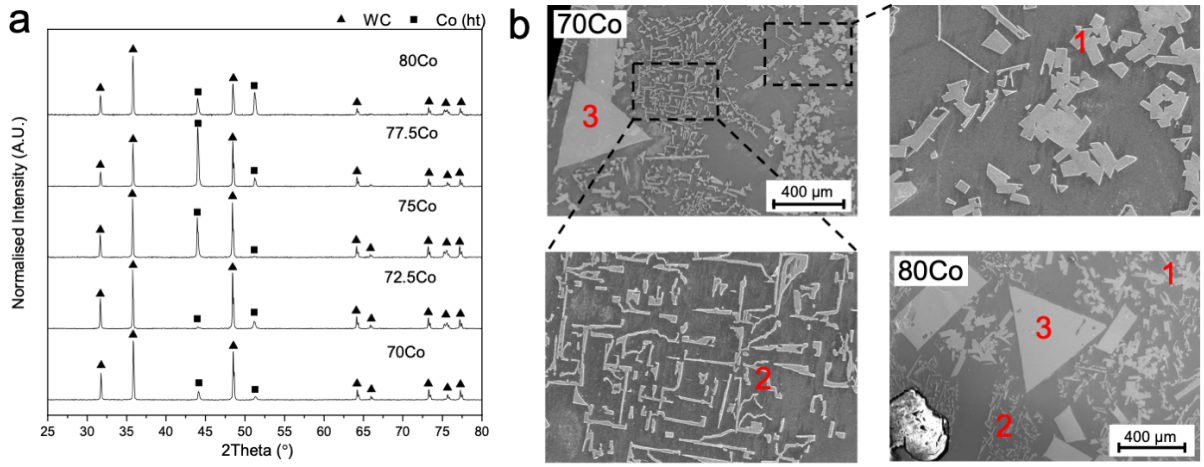

Fig. 2. Structure of the 70-80Co samples. (a) XRD spectra, peaks were identified as the WC and Co (ht) phase, as matched to international centre for diffraction data reference spectra. (b) SEM micrographs of two samples taken from the compositional extremes; WC-70Co and WC-80Co, showing the three WC grain populations: (1) facetted; (2) laths; and (3) abnormal.

1) *Medium sized grains:* The first grain population (1) are the smaller faceted WC grains, shown in the upper-right quadrant, with a size of ~10 µm, which were found throughout the volume. Their equiaxed shape means they will have likely formed homogeneously from the melt. Further evidence for this is found by comparing their size with samples grown at the same temperature, but with lower Co contents (<70 at.%), such that maximum temperature was in the L+WC region to ensure solution-precipitation based growth. In these samples the grain size was also ~ 10 µm also (see Supplementary Fig. 1 and Supplementary Table 1). Their similar size and shape suggests the same basic growth mechanism [34].

2) *Lath grains:* The second population of WC grains (2) are heavily elongated, forming a mesh-like pattern of interconnecting laths, as shown in the lower-left quadrant. The laths measured <10 µm along their shortest axis. The laths were generally found in proximity of abnormally large WC grains (3) with a thin layer of Co between. The laths appear to preferentially grow along certain crystallographic planes; which are presumably the $(10\bar{1}0)$ planes as is expected in WC [5]. This indicates they are the last solid to form, from a highly undercooled liquid.

3) *Abnormal grains:* The final population were abnormally large WC grains (3), hereafter defined as those >100 µm in the long-axis direction. Sample WC-80Co showed these grains throughout its volume. However, at lower Co contents they were found predominantly near the upper surface region, (i.e. near the furnace gas-melt interface). This is likely related to the faster cooling at the surface compared to the bulk. In order to elucidate the growth mechanism behind these abnormal grains, further evidence is needed from samples grown at the eutectic composition.

Fig. 3(a) shows SEM micrographs of the eutectic composition (WC-83Co) samples grown with various final hold temperatures of 1200, 1300 and 1400 ˚C respectively. All samples show abnormal WC grains. However, the T1200 and T1400 samples also contained graphite and the η-phase (Co_4W_2C), in addition to those phases in the starting powder mixture. Supporting XRD patterns for graphite and η-phase are shown in supplementary Fig. 2. The η-

phase was formed in dendritic patterns. By contrast, T1300 shows no η-phase or graphite and instead a WC lath microstructure, similar to that in Fig. 2. The homogeneously grown microstructure was not observed in any samples.

Fig. 3b shows a boxplot of the grain size distributions. When comparing the maximum size of abnormally large WC grains (indicated by red dot in Fig. 3(b)), the T1300 sample showed the largest (~7 mm), which coincided with the absence of η-phase. The T1200 sample had the smallest (~2 mm), with significant remnant η-phase. Finally, in T1400, only two unambiguous WC grains were found in the sample, both 3-4 mm in size. Furthermore, there were also multiple regions of WC that appeared to be growing from the dendritic η-phase regions, as shown in the upper right micrograph of Fig. 3(a). Since they were not distinct grains, being connected to η-phase, these regions were not counted in the size statistics, however they indicate a connection between WC growth and the η-phase.

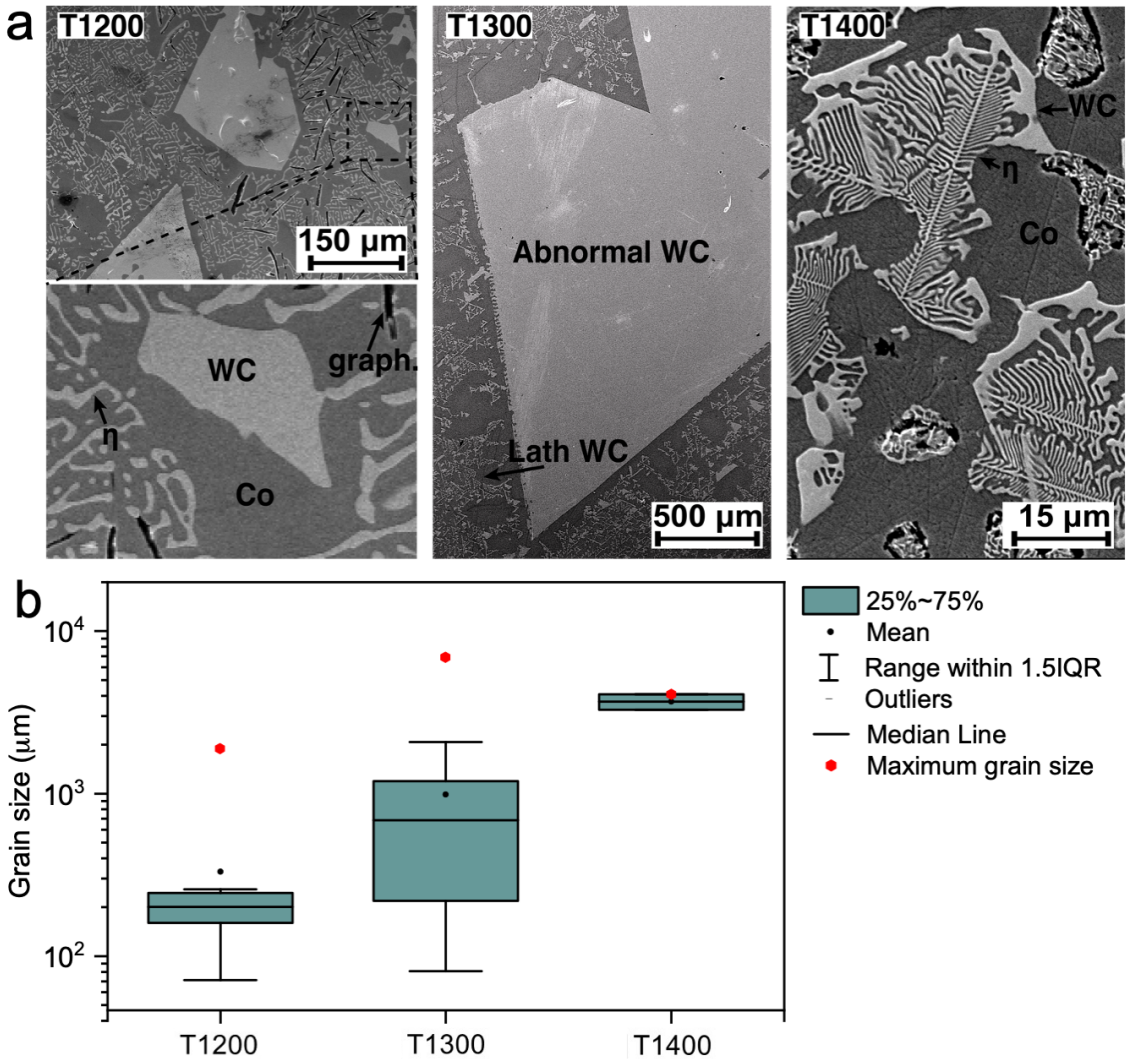

Fig. 3. Structure of the 83 Co samples. (a) SEM micrographs, showing the presence of dendritic η-phase in T1200 and T1400, and its absence in T1300. (b) Boxplot of abnormally large grains, showing the peak in maximum grain size at T1300.

A comparison of Figs. 2 and 3 reveals that the composition in which the η-phase is the first solid to form, i.e. ~83 at.%, also coincided with very largest abnormal grains. Furthermore, when the secondary hold was completed at 1300 ˚C, the η-phase was absent,

and the size of abnormal WC grains increased further. This evidence again points to η-phase formation being connected with abnormal growth. Fig. 4 explores this point further.

Fig. 4 correlates the secondary hold temperatures, and the corresponding microstructures in the eutectic samples, to the phase diagram. The T1400 hold is located in the L+η phase field. Thus, upon cooling from this field into the Co+WC one, after the completion of the secondary hold, the microstructure would have been rich in the η-phase. The reason for metastable η-phase formation is possibly due to its lower surface energy [34] compared to WC [35,36], meaning at relatively low undercoolings its formation would be energetically favored. The large WC grains can therefore be attributed to grow directly from the η-phase. Evidence for this is in the upper-right micrograph, which is reproduced in schematic form to its left.

Collating the evidence from Figs. 2-4, we propose that the abnormal growth occurs while η is carburised to form WC and expel Co, following the reaction:

$$Co_4W_2C + C \rightarrow 2WC + 4Co \quad (1)$$

We note that WC growth from the η-phase has been observed at much lower Co-contents of 10 wt.% [37], however such materials always retained a majority of solid WC, and the resulting WC grains were only a few microns across, not several mm, as observed here.

The lack of full η-phase carburisation in T1400 and T1200 can be explained by kinetic limitations. Since carburisation would require extensive mass transport [38], and the cooling from T1400 was relatively fast, the amount of transformation would be severely limited, resulting in a high fraction of η-phase, and only two abnormal WC grains.

The T1200 hold was located in the Co+WC phase field, with less time spent in the L+η phase field (<3h, vs. 10h for T1400), resulting in smaller η-phase regions. Therefore, the WC grains growing from this η-phase would be smaller and more numerous, as shown in the size statistics. Again, the cooling rate was too fast for complete transformation, resulting in retained η-phase.

By contrast, the T1300 secondary hold has the optimum growth conditions, as it is likely to be within the Liquid+Co+η phase field (although the phase field is narrow, so it is possible that liquid is not always present). This is the highest possible temperature at which there is a driving force for WC to form, leading to the fastest possible growth kinetics, and thus the full transformation of the η-phase, resulting in the largest abnormal WC grain population.

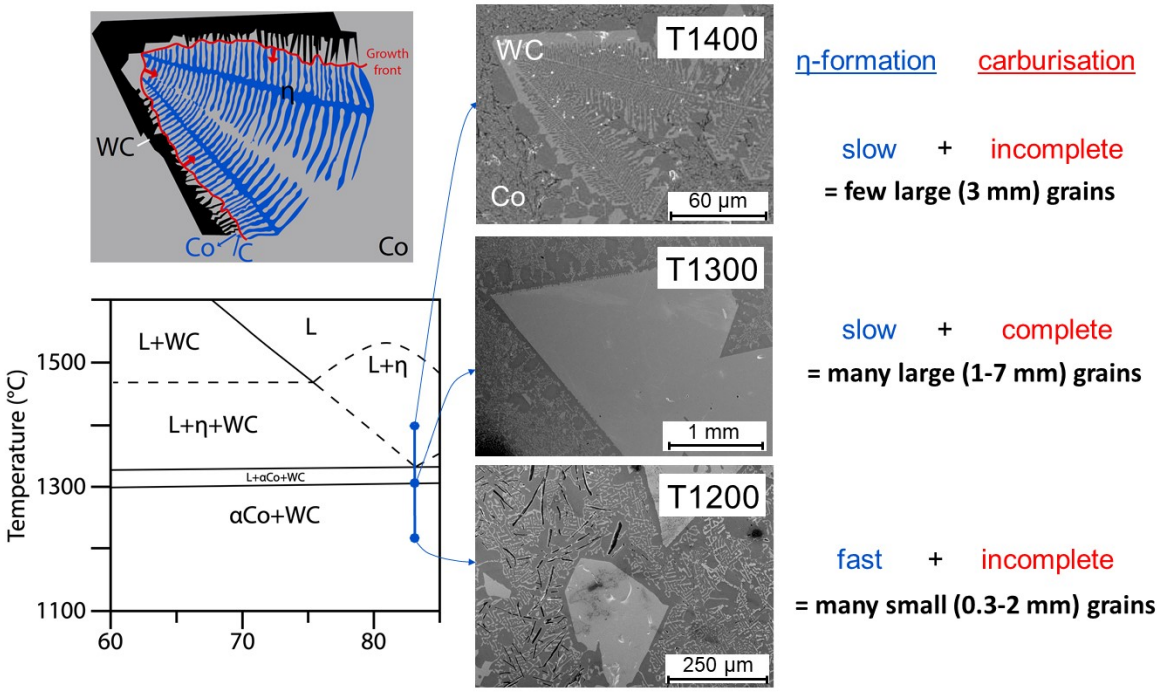

Fig. 4. Summary of microstructures formed at each secondary hold temperature, correlated to the phase diagram (lower left). The mechanism of WC growth from the decomposition of the dendritic η-to-WC transformation is drawn from the T1400 SEM image (upper left). The T1300 treatment was the only one that has both full development of η-phase formation, and adequate time for η-to-WC transformation, hence it showed optimum growth.

Given that the η-phase would have likely also formed in the sub-eutectic 70-80Co samples (see Fig. 1), it is logical to conclude that the abnormal grains found in these samples also formed via the carburisation reaction given in Eq. (1). The fact that they were smaller can be explained by the WC being the first solid to form (i.e. not η). Therefore, the amount of η-phase available for the WC → η-phase reaction would have been limited.

We now combine the grain size data from eutectic and sub-eutectic samples, shown in Fig. 5. The largest abnormal grains, indicated as red circles, tend to increase monotonically with increasing Co content, which can now be explained by the increase in η-phase formation. The size increased markedly beyond 75 at.%, marking the point at which η-phase is the first solid to form (see Fig. 1).

However, the average grain size, shown by black dots, does not show a monotonic trend. At lower Co contents of 70-75 at.%, the average size decreases with Co content, resulting in a local minimum at ~75 at.%. This can be explained by a second factor that controls the size of the smaller (i.e. non-abnormal) grains. This factor is the L→L+WC liquidus temperature, which decreases with Co content. For example, between 72.5-75 at.% Co, the liquidus decrease in Fig. 1 is ~80 °C. The liquidus controls the rates of diffusion in the semi-solid state [39], [40]. Thus, as the liquidus temperature decreases, the rate of WC growth decreases.

These opposing factors result in two regimes of average grain size variation:

1) *Low Co (<75 at.%) regime of homogenous nucleation controlled by the liquidus*. As Co content increases, the liquidus temperature decreases, which leads to nucleation of WC at a lower temperature, and thus slower growth.

2) *High Co (>75 at.%) regime controlled by η-phase carburisation in abnormal grains.* As Co content increases, the content of η-phase is increased, therefore the size and number of the largest WC crystals also increases.

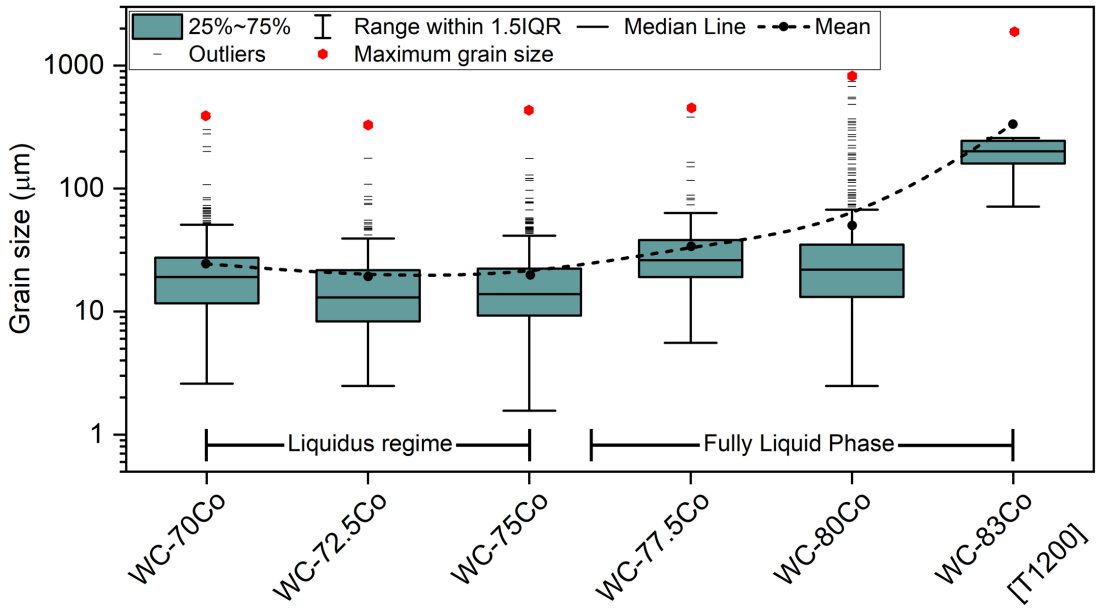

Fig. 5. Grain size box-plot for samples processed using the T1200 heat treatment at different cobalt contents. At low Co contents the grain size is controlled by the liquidus temperature, while at higher the grain size is controlled by the volume fraction of parent η-phase.

Before concluding the results of this study it is worth noting that the carburisation reaction mechanism may be applicable to WC growth from other metal fluxes that also form η-phase, e.g. Fe and Ni [41], [42]. It may also be applicable to the growth of other metal carbides, e.g. MoC, which also adopts a hexagonal monocarbide structure, forms an analogous ternary η-phase, and shows relatively sluggish diffusion.

4. Conclusions

In summary, the mechanism of macroscale (several mm) WC crystal growth from Co-rich liquid flux has been shown to occur from decomposition of the η-phase.

Such large crystal growth is therefore most easily achieved at the eutectic composition, 83 at.% Co, where it is the first solid to form. Whether any η-phase remained in the microstructure depended on the cooling rate. When cooled slowly through the L+Co+η→Co+WC phase transformation, at ~1300 ˚C, the η-phase transformed completely and the WC grain size was maximised. However, when cooling through this phase transition was more rapid, η-phase and graphite were retained, and the abnormal grains were smaller.

At sub-eutectic compositions, a combination of the above mechanisms was observed, i.e. some abnormal growth from regions of η-phase and some normal grain growth of homogenously nucleated WC.

The proposed reaction mechanism may be applicable to other carbide ceramics, e.g. MoC and to other metal fluxes, e.g. Fe and Ni.

Based on the above developments, some recommendations for the targeted growth of large WC single crystals can be made: (i) the content of η-phase prior to the decomposition at

~1300 ˚C should be maximised, by processing at the eutectic composition; and (ii) the cooling rate through the L+Co+η→Co+WC phase transformation at ~1300 ˚C must be as slow as possible. This new mechanistic understanding may facilitate meso-scale tests to be applied to such crystals in future.

Data availability

The raw data required to reproduce these findings will be made available on request.

Acknowledgements

SHB was financially supported by the Imperial College Research Fellowship.

References

[1] P. Ettmayer, "Hardmetals and cermets," *Annu. Rev. Mater. Sci.*, vol. 19, no. 1, pp. 145–164, Aug. 1989.
[2] Z. Z. Fang, M. C. Koopman, and H. Wang, "Cemented tungsten carbide hardmetal - An introduction," in *Comprehensive Hard Materials*, Elsevier, 2014, pp. 123–137.
[3] T. Takahashi and E. J. Freise, "Determination of the slip systems in single crystals of tungsten monocarbide," *Philos. Mag.*, vol. 12, no. 115, pp. 1–8, Jul. 1965.
[4] X. Liu, H. Wang, X. Song, and Q. Zhang, "Indentation-Induced Deformation of Ultracoarse Grained Cemented Carbides," 2016.
[5] S. Lay, P. Donnadieu, and M. Loubradou, "Polarity of prismatic facets delimiting WC grains in WC-Co alloys," in *Micron*, vol. 41, no. 5, Pergamon, 2010, pp. 472–477.
[6] I. M. Lifshitz and V. V. Slyozov, "The kinetics of precipitation from supersaturated solid solutions," *J. Phys. Chem. Solids*, vol. 19, no. 1–2, pp. 35–50, Apr. 1961.
[7] S. Lay, J. Vicens, and F. Osterstock, "High temperature creep of WC-Co alloys," 1987.
[8] M. A. Yousfi, J. Weidow, A. Nordgren, L. K. L. Falk, and H.-O. Andrén, "Deformation mechanisms in a WC-Co based cemented carbide during creep," *Int. J. Refract. Met. Hard Mater.*, vol. 49, pp. 81–87, Mar. 2015.
[9] D. Mari, S. Bolognini, T. Viatte, and W. Benoit, "Study of the mechanical properties of TiCN-WC-CO hardmetals by the interpretation of internal friction spectra," *Int. J. Refract. Met. Hard Mater.*, vol. 19, no. 4–6, pp. 257–265, Jul. 2001.
[10] K. Buss, "High temperature deformation mechanisms of cemented carbides and cermets," EPFL, 2004.
[11] J. Weidow, "Effect of metal and cubic carbide additions on interface chemistry, phase composition and grain growth in WC-Co based cemented carbides," Chalmers University of Technology, 2010.
[12] M. Christensen and G. Wahnström, "Strength and reinforcement of interfaces in cemented carbides," *Int. J. Refract. Met. Hard Mater.*, vol. 24, no. 1–2, pp. 80–88, Jan. 2006.
[13] M. Christensen and G. Wahnström, "Effects of cobalt intergranular segregation on interface energetics in WC-Co," *Acta Mater.*, vol. 52, no. 8, pp. 2199–2207, May 2004.
[14] M. A. Yousfi, S. Norgren, H.-O. Andrén, and L. K. L. Falk, "Chromium segregation at phase boundaries in Cr-doped WC-Co cemented carbides," *Mater. Charact.*, vol. 144, pp. 48–56, Oct. 2018.
[15] T. Csanádi, M. Bľanda, A. Duszová, N. Q. Chinh, P. Szommer, and J. Dusza, "Deformation characteristics of WC micropillars," *J. Eur. Ceram. Soc.*, vol. 34, no. 15, pp. 4099–4103, Dec. 2014.
[16] J. M. Tarragó, J. J. Roa, E. Jiménez-Piqué, E. Keown, J. Fair, and L. Llanes, "Mechanical deformation of WC-Co composite micropillars under uniaxial compression," *Int. J. Refract. Met. Hard Mater.*, vol. 54, pp. 70–74, Jul. 2016.

[17] D. A. Sandoval, A. Rinaldi, J. M. Tarragó, J. J. Roa, J. Fair, and L. Llanes, “Scale effect in mechanical characterization of WC-Co composites,” *Int. J. Refract. Met. Hard Mater.*, vol. 72, pp. 157–162, Apr. 2018.
[18] T. Klünsner *et al.*, “Effect of specimen size on the tensile strength of WC-Co hard metal,” *Acta Mater.*, vol. 59, no. 10, pp. 4244–4252, Jun. 2011.
[19] M. Trueba *et al.*, “‘In-situ’ mechanical characterisation of WC-Co hardmetals using microbeam testing,” *Int. J. Refract. Met. Hard Mater.*, vol. 43, pp. 236–240, Mar. 2014.
[20] D. E. J. Armstrong, A. J. Wilkinson, and S. G. Roberts, “Micro-mechanical measurements of fracture toughness of bismuth embrittled copper grain boundaries,” *Philos. Mag. Lett.*, vol. 91, no. 6, pp. 394–400, Jun. 2011.
[21] N. Jaya B, V. Jayaram, and S. K. Biswas, “A new method for fracture toughness determination of graded (Pt,Ni)Al bond coats by microbeam bend tests,” *Philos. Mag.*, vol. 92, no. 25–27, pp. 3326–3345, Sep. 2012.
[22] S. Liu, J. M. Wheeler, P. R. Howie, X. T. Zeng, J. Michler, and W. J. Clegg, “Measuring the fracture resistance of hard coatings,” *Appl. Phys. Lett.*, vol. 102, no. 17, p. 171907, Apr. 2013.
[23] G. Sernicola *et al.*, “In situ stable crack growth at the micron scale,” *Nat. Commun.*, vol. 8, no. 1, p. 108, Dec. 2017.
[24] R. J. Nelson and D. R. Milner, “Densification processes in the tungsten carbide-cobalt system,” *Powder Metall.*, vol. 15, no. 30, pp. 346–363, Sep. 1972.
[25] C. Wagner, “Theorie der Alterung von Niederschlägen durch Umlösen (Ostwald-Reifung),” *Zeitschrift für Elektrochemie, Berichte der Bunsengesellschaft für Phys. Chemie*, vol. 65, no. 7–8, pp. 581–591, 1961.
[26] B.-K. Yoon, B.-A. Lee, and S.-J. L. Kang, “Growth behavior of rounded (Ti,W)C and faceted WC grains in a Co matrix during liquid phase sintering,” *Acta Mater.*, vol. 53, no. 17, pp. 4677–4685, Oct. 2005.
[27] A. P. Gerk and J. J. Gilman, “Growth of Tungsten Carbide Monocrystals,” *J. Appl. Phys.*, vol. 39, no. 10, pp. 4497–4500, Sep. 1968.
[28] H.-O. Andrén, “Microstructures of cemented carbides,” *Mater. Des.*, vol. 22, no. 6, pp. 491–498, Sep. 2001.
[29] H.-O. Andrén, “Microstructure development during sintering and heat-treatment of cemented carbides and cermets,” *Mater. Chem. Phys.*, vol. 67, no. 1–3, pp. 209–213, Jan. 2001.
[30] G. S. Upadhyaya, *Cemented tungsten carbides: production, properties, and testing*. Noyes Publications, 1998.
[31] Pauling File Multinaries, “C-Co-W Vertical Section of Ternary Phase Diagram.” Springer-Verlag Berlin Heidelberg & Material Phases Data System (MPDS), Switzerland & National Institute for Materials Science (NIMS), Japan, 2012.
[32] A. Bondar, N. Bochvar, T. Dobatkina, N. Krendelsberger, and M. Materials Science International Team, “C-Co-W ternary phase diagram evaluation.” MSI Materials Science International Services GmbH.
[33] B. Roebuck and E. G. Bennett, “The metallographic measurement of WC grain size.”
[34] Christensen, M., Wahnström, G., Lay, S., Allibert, C. "Morphology of WC grains in WC–Co alloys: Theoretical determination of grain shape," *Acta Mater.*, vol. 55, no. 5, pp. 1515-1521, Mar. 2007.
[35] R. Warren, "Determination of the interfacial energy ratio in two-phase systems by measurement of interphase contact," *Metallography*, vol. 9, no. 3, pp. 183-191, Jun. 1976.
[36] Christensen, M., Wahnström, " Effects of cobalt intergranular segregation on interface energetics in WC–Co", *Acta Mater.*, vol. 52, no. 8, pp. 2199-2207, May 2004.
[37] A. Adorjan, W. D. Schubert, A. Schön, A. Bock, and B. Zeiler, “WC grain growth during the early stages of sintering,” *Int. J. Refract. Met. Hard Mater.*, vol. 24, no. 5, pp. 365–373, Sep. 2006.
[38] S. Lay and M. Loubradou, “Characteristics and origin of clusters in submicron WC-Co cermets,” *Philos. Mag.*, vol. 83, no. 23, pp. 2669–2679, Aug. 2003.
[39] M. Leiderman, A. Rosen, and O. Botstein, “Proceedings of Euro PM 96,” 1996.
[40] P. Arató, L. Bartha, R. Porat, S. Berger, and A. Rosen, “Solid or liquid phase sintering of nanocrystalline WC/Co hardmetals,” *Nanostructured Mater.*, vol. 10, no. 2–8, pp. 245–255,

Feb. 1998.
[41] C. M. Fernandes and A. M. R. Senos, “Cemented carbide phase diagrams: A review,” *International Journal of Refractory Metals and Hard Materials*, vol. 29, no. 4. Elsevier, pp. 405–418, 01-Jul-2011.
[42] C. M. Fernandes, A. M. R. Senos, and M. T. Vieira, “Control of eta carbide formation in tungsten carbide powders sputter-coated with (Fe/Ni/Cr),” *Int. J. Refract. Met. Hard Mater.*, vol. 25, no. 4, pp. 310–317, Jul. 2007.